

Supporting Information

Synergistic construction of highly symmetrical lanthanide single-ion magnets using neutral phosphoryl and anionic thiocyanate ligands

Bei Liu,^{‡,a} Xiao-Yan Dong,^{‡,a} Hui-Wen Gong,^a Zheng Sun,^c Rong Sun,^c Wen-Hua Zhu,^{*,a} Lei Zhang,^b Hao-Ling Sun,^{*,b} Man-Yun Zhao,^a Ning-Ning Huang,^a Qing-Yan Bian^a and Song Gao^{*,c}

^aCollaborative Innovation Center for Advanced Organic Chemical Materials Co-constructed by the Province and Ministry, Ministry-of-Education Key Laboratory for the Synthesis and Application of Organic Functional Molecules, College of Chemistry and Chemical Engineering, Hubei University, Wuhan 430062, P. R. China.

^bDepartment of Chemistry and Beijing Key Laboratory of Energy Conversion and Storage Materials, Beijing Normal University, Beijing 100875, P. R. China.

^cBeijing National Laboratory for Molecular Sciences, State Key Laboratory of Rare Earth Materials Chemistry and Applications, College of Chemistry and Molecular Engineering, Peking University, No. 5 Yiheyuan Road, Beijing 100871, P. R. China.

Email: zhuwenhua@hubu.edu.cn; Email: haolingsun@bnu.edu.cn;
Email: gaosong@pku.edu.cn.

1. Experimental Section

Materials and physical techniques

Unless otherwise stated, all chemicals and solvents were of analytical reagent grade and used as purchased without further purification. All reactions were carried out under aerobic conditions. Elemental analyses of C, H and N were carried out on an elementar UNICUBE (**1** and **2**) or Vario Micro Cube (**3** and **4**) elemental analyzer (Elementar Aanlysensysteme GmbH, Germany). IR spectra (4000–400 cm⁻¹) on powdered samples were recorded on a Perkin Elmer Spectrum one spectrophotometer using KBr pellets. Powder X-ray diffraction (PXRD) data for the as-prepared samples were collected on a D8 ADVANCE (Bruker AXS, Germany) diffractometer at room temperature using Cu-K α radiation.

X-ray crystallography

Determination of the unit cell and data collection for complexes **1–4** at the corresponding temperatures were performed on a Bruker Smart APEX II CCD area detector diffractometer (**1**) with graphite-monochromated Mo K α radiation ($\lambda = 0.71073 \text{ \AA}$), a rigaku SuperNova, Dual, AtlasS2 diffractometer (**2**) with graphite-monochromated Cu K α radiation ($\lambda = 1.54184 \text{ \AA}$) and Rigaku XtaLAB Synergy four-circle diffractometer with graphite-monochromated Cu-K α radiation (**3**, $\lambda = 1.54184 \text{ \AA}$) and Mo K α radiation (**4**, $\lambda = 0.71073 \text{ \AA}$). All of the diffraction data were collected at room temperature and corrected for Lorentz and polarization effects. Adsorption corrections were applied by SADABS method.¹ Using Olex2,² the structures were solved by heavy (**1**), dual (**2**) or direct (**3** and **4**) methods of SHELXS-2008 program and refined by the full-matrix least-squares techniques based on F^2 using SHELXL-2014 program.^{3a,b}

With the very helpful work of the crystallographer reviewer, we have processed these compounds using disorder models, improving the quality of the data. For compound **1**, the morpholine ring containing N9 atom is disordered in two positions, so it has been refined based on the disorder model. For compound **2**, the two morpholine rings respectively containing N7 and N11 atom are disordered in two positions, so they have been refined based on the disorder model. For compound **3**, S1 atom and the morpholine ring containing N9 atom are respectively disordered in two positions, so they have been refined based on the disorder model. For compound **4**, the PF₆⁻ anion, the P(NMe₂)₃ groups of the two HMPA ligands involving P1 and P3 are disordered, so they have been refined based on the disorder model. The P(NMe₂)₃ groups of the other two HMPA ligands involving P2 and P4 are likely slightly disordered based on the ADPs (atomic displacement parameters), but it was less apparent than the previous two, thus no disordered processing was carried out.

Due to the relatively poor crystal quality and disordered components in compound **4**, the quality of the crystal data collected at room temperature is relatively poor ($R_{\text{int}} = 0.1304$), and the structural

refinement results showed that the R_1 (0.1233) and wR_2 (0.3088) factors were relatively high with only empirical absorption correction (multi-scan). Therefore, we recollected the data at a low temperature of 150 K, combined empirical absorption correction using spherical harmonics (SCALE3 ABSPACK) and numerical absorption correction based on gaussian integration over a multifaceted crystal model to reduce the R_{int} (0.1208) value, and improved the structural refinement results ($R_1 = 0.0929$, $wR_2 = 0.2295$).

All of the ordered non-hydrogen atoms were refined with anisotropic thermal parameters. Hydrogen atoms of the coordinated and lattice H₂O molecules were located by difference Fourier map and refined isotropically with constrains for the ideal geometry of H₂O molecules with an O–H distance of 0.96 Å and an H–O–H angle of 105°. Organic hydrogen atoms were introduced on calculated positions and refined with isotropic thermal parameters and a fixed geometry riding on their parent atoms.^{3c,d}

The crystal data and structural refinement details of **1–4** are respectively summarized in Table S1. The selected bond lengths and angles of **1–4** are listed in Tables S2–S8 in the ESI. CCDC 2422425–2422428.

Magnetic measurement

Static magnetic measurements including temperature-dependent magnetic susceptibility in the range of 2–300 K, and field-dependent magnetization, ac susceptibilities of **1** and **2** (1–1000 Hz) were carried out on a Quantum Design MPMS-XL5 SQUID magnetometer. All magnetic measurements were performed on polycrystalline samples tightly packed with grease and sealed with film to avoid the anisotropic orientation. Diamagnetic corrections were made with Pascal's constants for all the constituent atoms.⁴

2. Structural Data and Diagram

Table S1 Crystallographic data for the complexes **1–4**

	1	2	3	4
Empirical formula	C ₂₇ H ₅₂ N ₉ O ₁₀ P ₂ S ₃ Dy	C ₅₄ H ₁₁₀ N ₁₈ O ₂₃ P ₄ S ₆ Dy ₂ C ₂₇ H ₅₂ N ₉ O ₁₀ P ₂ S ₃ Ho	C ₂₆ H ₇₂ N ₁₄ O ₄ F ₆ P ₅ S ₂ Dy	
Formula weight	983.39	2020.83	985.82	1140.44
Temperature/K	286.1	100.15	153.15	150.15
Crystal system	triclinic	monoclinic	triclinic	Orthorhombic
Space group	$\bar{P}1$	$P2_1/c$	$\bar{P}1$	$Pbca$
<i>a</i> [Å]	10.0947(4)	19.7170(4)	10.08750(10)	26.6565(13)
<i>b</i> [Å]	13.1152(5)	24.9048(5)	13.10110(10)	24.4382(11)
<i>c</i> [Å]	17.2101(7)	17.7571(3)	17.17690(10)	16.7250(7)
α [°]	69.7420(10)	90	69.6750(10)	90
β [°]	73.8000(10)	103.526(2)	73.7700(10)	90
γ [°]	86.7990(10)	90	86.7580(10)	90
Volume [Å ³]	2050.60(14)	8477.7(3)	2041.81(3)	10895.3(9)
<i>Z</i>	2	4	2	8
<i>D</i> _c [g cm ⁻³]	1.593	1.583	1.603	1.391
Radiation	Mo <i>K</i> α ($\lambda = 0.71073$)	Cu <i>K</i> α ($\lambda = 1.54184$)	Cu <i>K</i> α ($\lambda = 1.54184$)	Mo <i>K</i> α ($\lambda = 0.71073$)
μ [mm ⁻¹]	2.113	12.068	6.311	1.657
<i>F</i> (000)	1002	4128	1004	4680
Total reflections collected	24503	70764	27957	53430
Uniq reflections	7506	17124	8229	9814
<i>R</i> _{int}	0.0345	0.0821	0.0406	0.1208
No. of refined parameters	520	1030	530	665
<i>R</i> 1 [$I \geq 2\sigma(I)$]	0.0284	0.0437	0.0323	0.0929
<i>wR</i> 2 (all data)	0.0649	0.1106	0.0823	0.2295
Goodness of fit	1.046	1.056	1.030	1.092

Table S2 Selected bond lengths (\AA) and angles ($^\circ$) for **1**

Dy(1)–O(1)	2.244(2)	Dy(1)–O(2)	2.280(2)
Dy(1)–O(3)	2.359(3)	Dy(1)–O(4)	2.398(3)
Dy(1)–N(1)	2.385(3)	Dy(1)–N(2)	2.412(3)
Dy(1)–N(3)	2.426(3)		
O(1)–Dy(1)–O(2)	163.19(9)	O(1)–Dy(1)–O(3)	92.44(9)
O(1)–Dy(1)–O(4)	122.14(10)	O(1)–Dy(1)–N(1)	81.54(10)
O(1)–Dy(1)–N(2)	82.81(10)	O(1)–Dy(1)–N(3)	76.24(10)
O(2)–Dy(1)–O(3)	79.59(9)	O(2)–Dy(1)–O(4)	74.26(10)
O(2)–Dy(1)–N(1)	82.27(10)	O(2)–Dy(1)–N(2)	99.01(10)
O(2)–Dy(1)–N(3)	115.82(10)		
O(3)–Dy(1)–N(1)	77.20(11)	N(1)–Dy(1)–N(2)	80.82(12)
N(2)–Dy(1)–O(4)	76.51(12)	O(4)–Dy(1)–N(3)	70.41(11)
N(3)–Dy(1)–O(3)	77.68(12)		

Symmetry codes: #1 $-x+1, -y+2, -z+1$; #2 $-x+1, -y+1, -z+2$; #3 $x+1, y, z$.**Table S3** Hydrogen bonding geometry for **1**: lengths (\AA) and angles ($^\circ$)

D–H \cdots A	d(D–H)	d(H \cdots A)	d(D \cdots A)	\angle (DHA)
O(3)–H(3A) \cdots O(8)#2	0.947(19)	1.78(2)	2.718(4)	170(5)
O(3)–H(3B) \cdots O(6)#3	0.944(19)	1.779(19)	2.714(4)	170(4)
O(4)–H(4A) \cdots O(7)#1	0.944(19)	1.85(2)	2.790(4)	177(5)
O(4)–H(4B) \cdots S(2)#1	0.945(19)	2.37(2)	3.313(3)	174(5)

Symmetry codes: #1 $-x+1, -y+2, -z+1$; #2 $-x+1, -y+1, -z+2$; #3 $x+1, y, z$.

Table S4 Selected bond lengths (Å) and angles (°) for **2**

Dy(1)–O(1)	2.248(3)	Dy(1)–O(2)	2.255(3)
Dy(1)–O(5)	2.350(3)	Dy(1)–O(6)	2.361(3)
Dy(1)–N(1)	2.396(4)	Dy(1)–N(2)	2.409(3)
Dy(1)–N(3)	2.406(3)		
O(1)–Dy(1)–O(2)	174.62(10)	O(1)–Dy(1)–O(5)	81.82(10)
O(1)–Dy(1)–O(6)	84.02(10)	O(1)–Dy(1)–N(1)	93.26(12)
O(1)–Dy(1)–N(2)	100.02(11)	O(1)–Dy(1)–N(3)	92.86(12)
O(2)–Dy(1)–O(5)	94.67(10)	O(2)–Dy(1)–O(6)	96.31(10)
O(2)–Dy(1)–N(1)	81.75(11)	O(2)–Dy(1)–N(2)	82.58(12)
O(2)–Dy(1)–N(3)	92.34(11)		
O(5)–Dy(1)–N(2)	71.16(11)	N(2)–Dy(1)–N(3)	75.88(12)
N(3)–Dy(1)–O(6)	72.00 (11)	O(6)–Dy(1)–N(1)	72.49(10)
N(1)–Dy(1)–O(5)	71.90(10)		
Dy(2)–O(3)	2.211(2)	Dy(2)–O(4)	2.246(2)
Dy(2)–O(7)	2.356(3)	Dy(2)–O(8)	2.388(3)
Dy(2)–O(9)	2.407(3)	Dy(2)–N(4)	2.376(4)
Dy(2)–N(5)	2.386(3)		
O(3)–Dy(2)–O(4)	173.21(9)	O(3)–Dy(2)–O(7)	85.42(10)
O(3)–Dy(2)–O(8)	83.56(9)	O(3)–Dy(2)–O(9)	88.99(10)
O(3)–Dy(2)–N(4)	97.83(11)	O(3)–Dy(2)–N(5)	97.98 (11)
O(4)–Dy(2)–O(7)	101.04(10)	O(4)–Dy(2)–O(8)	89.80(9)
O(4)–Dy(2)–O(9)	87.49(9)	O(4)–Dy(2)–N(4)	82.31(11)
O(4)–Dy(2)–N(5)	86.31(11)		
O(7)–Dy(2)–N(4)	72.42 (11)	N(4)–Dy(2)–O(8)	79.64(11)
O(8)–Dy(2)–O(9)	70.93 (9)	O(9)–Dy(2)–N(5)	70.51(10)
N(5)–Dy(2)–O(7)	69.79(10)		

Symmetry codes: #1 $-x+1, -y+1, -z+1$; #2 $x-1, y, z$; #3 $-x+1, -y+1, -z+2$; #4 $x, -y+3/2, z+1/2$; #5 $x+1, -y+3/2, z+1/2$; #6 $x+1, y, z$.

Table S5 Hydrogen bonding geometry for **2**: lengths (Å) and angles (°)

D–H···A	d(D–H)	d(H···A)	d(D···A)	<(DHA)
O(5)–H(5A)···O(23)#2	0.87	1.92	2.708(4)	149.7
O(5)–H(5B)···O(10)	0.87	1.91	2.705(4)	150.5
O(6)–H(6A)···O(15)#3	0.87	1.88	2.739(4)	169.1
O(6)–H(6B)···O(18)#4	0.87	1.94	2.761(4)	156.4
O(7)–H(7C)···O(16)#1	0.87	2.03	2.780(6)	143.6
O(8)–H(8C)···S(6)#5	0.90	2.32	3.177(3)	158.9
O(8)–H(8D)···O(19)#4	0.90	1.98	2.782(4)	148.3
O(9)–H(9C)···O(13)#6	0.88	2.19	2.800(4)	125.8
O(9)–H(9D)···O(11)#6	0.88	2.05	2.793(4)	142.0
O(10)–H(10E)···O(11)	0.87	1.99	2.846(4)	167.6
O(10)–H(10F)···O(22)#1	0.87	2.07	2.887(4)	156.5
O(11)–H(11C)···N(6)	0.87	1.90	2.757(5)	166.8
O(11)–H(11D)···S(5)#2	0.87	2.46	3.298(3)	161.8

Symmetry codes: #1 $-x+1, -y+1, -z+1$; #2 $x-1, y, z$; #3 $-x+1, -y+1, -z+2$; #4 $x, -y+3/2, z+1/2$; #5 $x+1, -y+3/2, z+1/2$; #6 $x+1, y, z$.

Table S6 Selected bond lengths (Å) and angles (°) for **3**

Ho(1)–O(1)	2.2322(15)	Ho(1)–O(2)	2.2680(14)
Ho(1)–O(3)	2.3434(17)	Ho(1)–O(4)	2.3809(18)
Ho(1)–N(1)	2.373(2)	Ho(1)–N(2)	2.394(2)
Ho(1)–N(3)	2.411(2)		
O(1)–Ho(1)–O(2)	163.21(6)	O(1)–Ho(1)–O(3)	92.45(6)
O(1)–Ho(1)–O(4)	122.28(7)	O(1)–Ho(1)–N(1)	81.44(7)
O(1)–Ho(1)–N(2)	82.83(7)	O(1)–Ho(1)–N(3)	76.29(7)
O(2)–Ho(1)–O(3)	79.54(6)	O(2)–Ho(1)–O(4)	74.12(6)
O(2)–Ho(1)–N(1)	82.40(7)	O(2)–Ho(1)–N(2)	99.01(7)
O(2)–Ho(1)–N(3)	115.68(7)		
O(3)–Ho(1)–N(1)	77.22(8)	N(1)–Ho(1)–N(2)	80.65(9)
N(2)–Ho(1)–O(4)	76.66(8)	O(4)–Ho(1)–N(3)	70.53(8)
N(3)–Ho(1)–O(3)	77.56(8)		

Symmetry codes: #1 $-x+1, -y+2, -z+1$; #2 $-x+1, -y+1, -z+2$; #3 $x+1, y, z$.

Table S7 Hydrogen bonding geometry for **3**: lengths (Å) and angles (°)

D–H···A	d(D–H)	d(H···A)	d(D···A)	<(DHA)
O(3)–H(3A)···O(8)#2	0.928(17)	1.799(19)	2.716(3)	170(4)
O(3)–H(3B)···O(6)#3	0.922(17)	1.793(17)	2.708(2)	171(3)
O(4)–H(4A)···O(7)#1	0.935(18)	1.858(19)	2.787(3)	172(4)
O(4)–H(4B)···S(2)#1	0.938(18)	2.38(2)	3.316(2)	172(4)

Symmetry codes: #1 $-x+1, -y+2, -z+1$; #2 $-x+1, -y+1, -z+2$; #3 $x+1, y, z$.

Table S8 Selected bond lengths (Å) and angles (°) for **4**

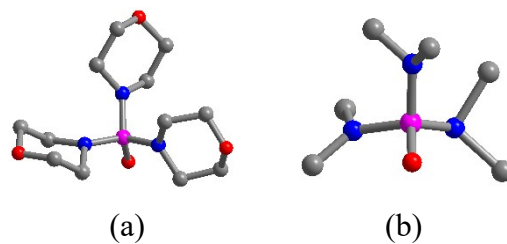
Dy(1)–O(1)	2.256(8)	Dy(1)–O(2)	2.247(7)
Dy(1)–O(3)	2.254(7)	Dy(1)–O(4)	2.238(7)
Dy(1)–N(1)	2.373(11)	Dy(1)–N(2)	2.394(10)
O(1)–Dy(1)–O(2)	169.0(3)	O(3)–Dy(1)–O(4)	168.6(3)
N(1)–Dy(1)–N(2)	178.4(4)		
N(1)–Dy(1)–O(1)	95.1(4)	N(1)–Dy(1)–O(2)	95.9(4)
N(1)–Dy(1)–O(3)	84.2(3)	N(1)–Dy(1)–O(4)	84.6(3)
N(2)–Dy(1)–O(1)	84.2(3)	N(2)–Dy(1)–O(2)	84.8(4)
N(2)–Dy(1)–O(3)	97.3(4)	N(2)–Dy(1)–O(4)	94.0(4)

Table S9 Continuous shape measures (CShM) for **1–3** using SHAPE 2.1

	HP-7	HPY-7	PBPY-7	COC-7	CTPR-7	JPBPY-7	JETPY-7
1	34.015	20.397	6.052	1.330	0.528	8.944	19.865
2 –Dy1	33.690	23.668	0.919	5.622	4.339	3.611	20.703
2 –Dy2	34.027	23.794	1.033	4.653	3.601	3.581	20.699
3	34.098	20.333	6.056	1.337	0.531	8.981	19.843

HP-7 = (D_{7h}) HeptagonCTPR-7 = (C_{2v}) Capped trigonal prismHPY-7 = (C_{6v}) Hexagonal pyramidJPBPY-7 = (D_{5h}) Johnson pentagonal bipyramid J13PBPY-7 = (D_{5h}) Pentagonal bipyramidJETPY-7 = (C_{3v}) Johnson elongated triangular pyramid J7COC-7 = (C_{3v}) Capped octahedron**Table S10** Continuous shape measures (CShM) for **4** using SHAPE 2.1

	HP-6	PPY-6	OC-6	TPR-6	JPPY-6
4	33.070	25.982	0.711	13.417	29.426

HP-6 = (D_{6h}) HexagonTPR-6 = (D_{3h}) Trigonal prismPPY-6 = (C_{5v}) Pentagonal pyramidJPPY-6 = (C_{5v}) Johnson pentagonal pyramid J2OC-6 = (O_h) Octahedron**Scheme S1.** Schematic structure of (a) TMPO and (b) HMPA molecules

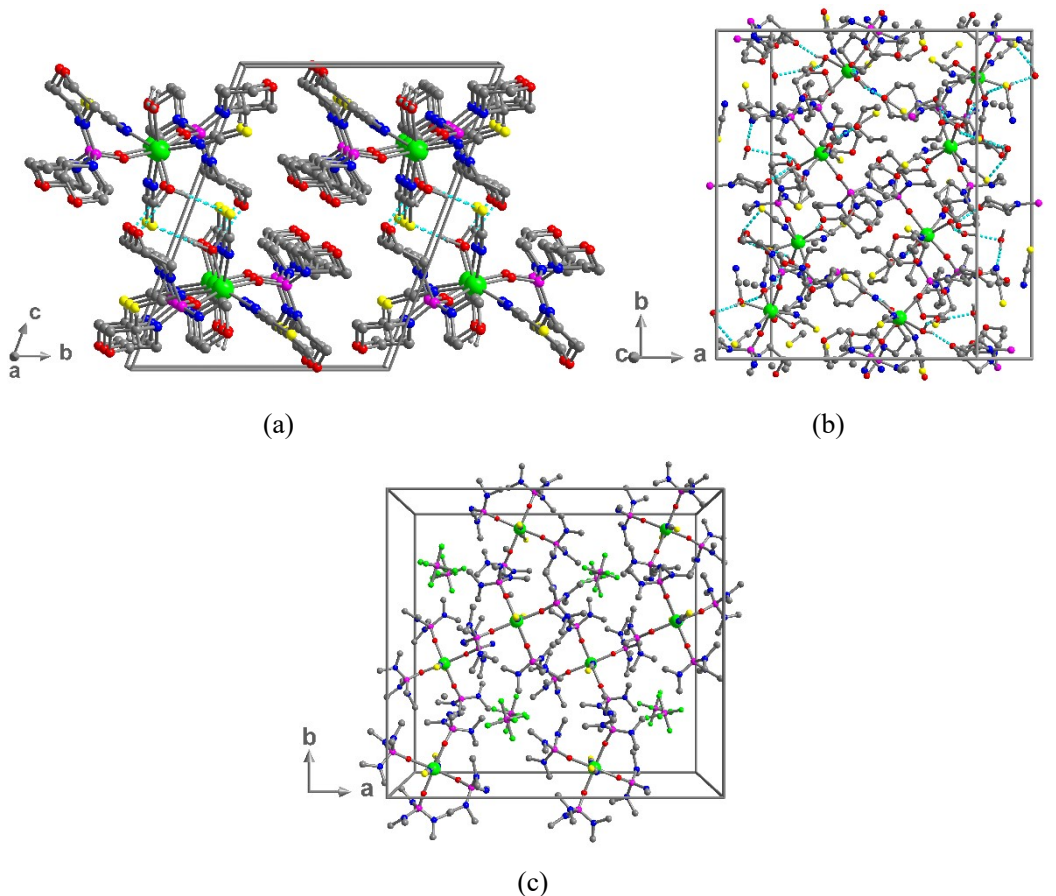
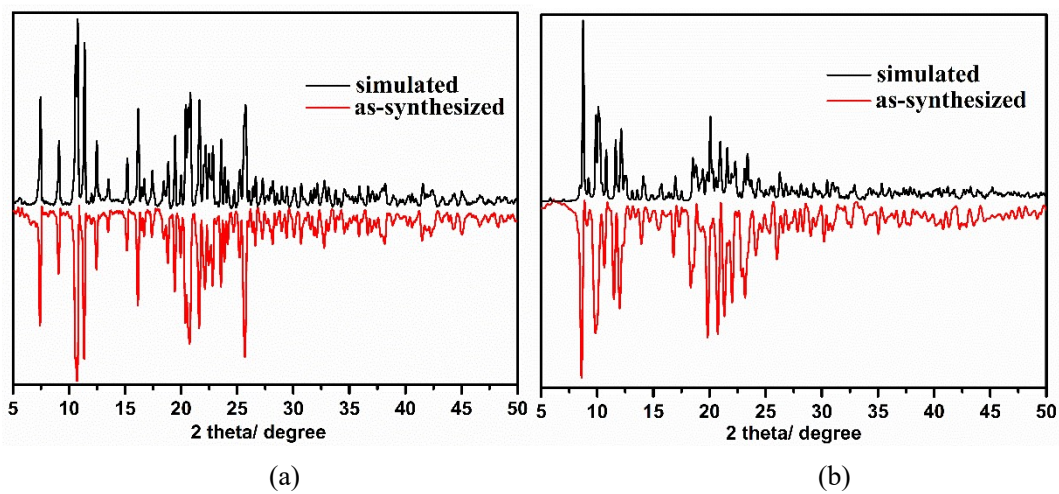
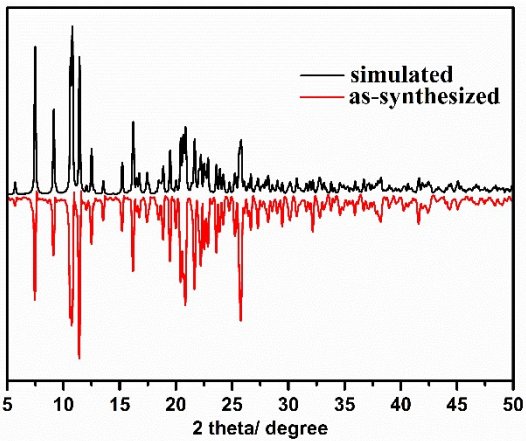


Fig. S1. (a) View of the packing pattern of compound **1** along the *a* direction. (b) View of the packing pattern of compound **2** along the *c* direction. (c) View of the packing pattern of compound **4** along the *c* direction. Color code: Dy, green; C, gray; N, blue; O, red; P, purple; S, yellow. Except for hydrogen bonding, all other hydrogen atoms are omitted for clarity.

3. Powder XRD Analyses

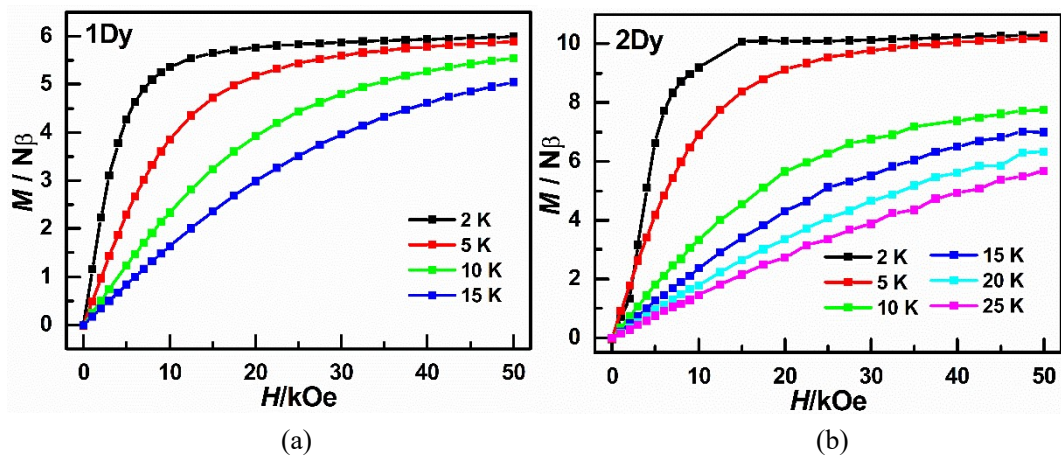




(c)

Fig. S2. Powder X-ray diffraction pattern of compounds (a) **1**, (b) **2** and (c) **3** for the as-synthesized sample and the simulated one.

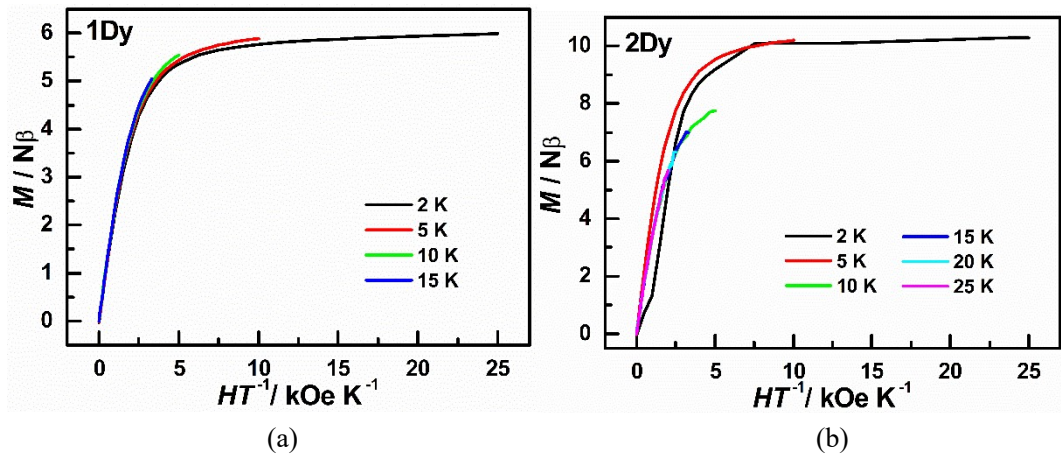
4. Magnetic Properties



(a)

(b)

Fig. S3. Field dependence of the magnetizations (a) for **1** at 2, 5, 10 and 15 K, and (b) for **2** at 2, 5, 10, 15, 20 and 25 K.



(a)

(b)

Fig. S4. Plots of the reduced magnetization M vs. H/T (a) for **1** at 2, 5, 10 and 15 K, and (b) for **2** at 2, 5, 10, 15, 20 and 25 K.

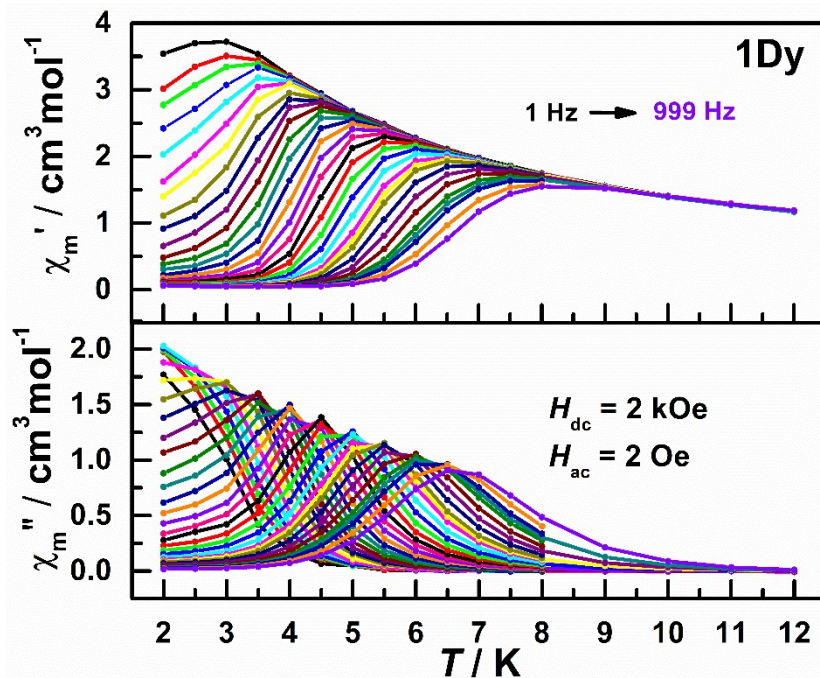


Fig. S5. Temperature dependence of the χ' and χ'' ac susceptibility components for compound **1** under a 2 kOe external dc field at indicated ac frequencies.

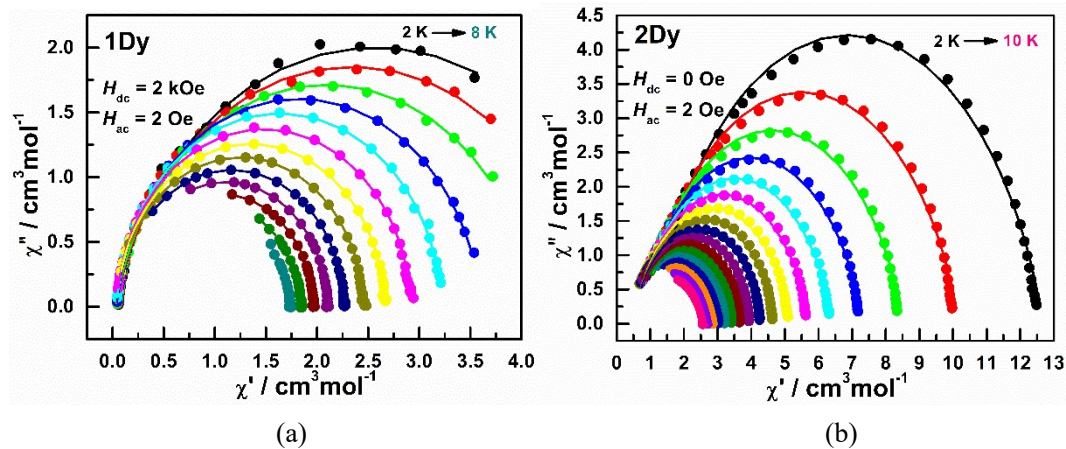


Fig. S6. The Cole–Cole plots (a) in the range of 2–8 K (0.5 K as a step) for **1** under a 2 kOe dc field and (b) in the range of 2–10 K (0.5 K as a step) for **2** under a 0 Oe dc field. The solid lines are the best fitting of the data to a distribution of single relaxation processes with the generalized Debye model.

Table S11 Relaxation parameters from the best fitting of the Cole–Cole diagrams in the range of 2–8 K by the generalized Debye model under a 2 kOe dc field for **1**.

T (K)	χ_s (cm ³ mol ⁻¹)	χ_t (cm ³ mol ⁻¹)	τ (s)	α
2.00	0.03	5.11	0.87E-1	0.068
2.50	0.03	4.77	0.61E-1	0.033
3.00	0.03	4.16	0.38E-1	0.013
3.50	0.04	3.61	0.18E-1	0.006
4.00	0.04	3.23	0.80E-2	0.004
4.50	0.04	2.92	0.34E-2	0.003
5.00	0.04	2.67	0.16E-2	0.003
5.50	0.05	2.45	0.76E-3	0.003
6.00	0.07	2.27	0.40E-3	0.001
6.50	0.11	2.10	0.23E-3	0.001
7.00	0.16	1.97	0.14E-3	0.000
7.50	0.16	1.85	0.87E-4	0.001
8.00	0.06	1.74	0.50E-4	0.001

Table S12 Relaxation parameters from the best fitting of the Cole–Cole diagrams in the range of 2–10 K by the generalized Debye model under a 0 Oe dc field for **2**.

T (K)	χ_s (cm ³ mol ⁻¹)	χ_t (cm ³ mol ⁻¹)	τ (s)	α
2.00	1.10	12.68	0.25E-2	0.20
2.50	0.89	10.17	0.25E-2	0.20
3.00	0.75	8.51	0.25E-2	0.20
3.50	0.65	7.32	0.25E-2	0.20
4.00	0.58	6.43	0.24E-2	0.20
4.50	0.52	5.73	0.23E-2	0.20
5.00	0.48	5.18	0.21E-2	0.20
5.50	0.46	4.72	0.18E-2	0.21
6.00	0.47	4.33	0.15E-2	0.21
6.50	0.49	4.00	0.12E-2	0.20
7.00	0.51	3.70	0.88E-3	0.19
7.50	0.51	3.45	0.61E-3	0.19
8.00	0.50	3.23	0.40E-3	0.20
8.50	0.53	3.04	0.28E-3	0.21
9.00	0.59	2.87	0.20E-3	0.21
9.50	0.67	2.72	0.15E-3	0.21
10.00	0.75	2.58	0.12E-3	0.22

5. Ab initio calculations

Complexes **1** and **2** are mononuclear compounds in the main structure, but there is one or two types of Dy^{III} fragments for each of them. Complete-active-space self-consistent field (CASSCF) calculations on individual Dy^{III} fragments (see Fig. 6 for the calculated model structures of complexes **1** and **2**) on the basis of single-crystal X-ray determined geometry have been carried out with MOLCAS 8.0 program package.⁵ During the calculation for **1** and **2**, the influence of distant Dy^{III} ions were taken into account by the closed-shell La^{III} *ab initio* embedding model potentials (AIMP; La.ECP.deGraaf.0s.0s.0e-La-(LaMnO₃)).

The basis sets for all atoms are atomic natural orbitals from the MOLCAS ANO-RCC library: ANO-RCC-VTZP for Dy^{III} or Er^{III} ion; VTZ for close O and N; VDZ for distant atoms. The calculations employed the second order Douglas-Kroll-Hess Hamiltonian, where scalar relativistic contractions were taken into account in the basis set and the spin-orbit couplings were handled separately in the restricted active space state interaction (RASSI-SO) procedure. For the fragment of an individual Dy^{III} or Er^{III} ion, active electrons in 7 active orbitals include all *f* electrons (CAS(9 in 7) for Dy^{III} fragments and CAS(11 in 7) for Er^{III} fragments) in the CASSCF calculation. To exclude all the doubts, we calculated all the roots in the active space. We have mixed the maximum number of spin-free states which was possible with our hardware (all from 21 sextets, 128 from 224 quadruplets, 130 from 490 doublets for Dy^{III} fragments; all from 35 quadruplets, all from 112 doublets for Er^{III} fragments). SINGLE_ANISO⁶⁻⁸ program was used to obtain the energy levels, *g* tensors, predominant *m_J* values, magnetic axes, *etc.*, based on the above CASSCF/RASSI-SO calculations.

Table S13. Calculated energy levels (cm^{-1}), \mathbf{g} (g_x , g_y , g_z) tensors and wavefunction compositions of the lowest eight Kramers doublets (KDs) of individual Dy^{III} fragments for compound **1**.

KDs	E/cm^{-1}	g_x	g_y	g_z	wavefunctions
1	0.0	0.246	0.664	19.002	90.5% ±15/2> + 4.8% ±11/2>
2	85.6	1.550	1.739	16.860	29.3% ±1/2> + 22.7% ±3/2> + 18.9% ±5/2>
3	152.8	2.044	5.719	11.230	56.8% ±13/2> + 12.0% ±1/2> + 12.0% ±3/2>
4	223.3	1.263	5.561	10.951	24.3% ±1/2> + 17.0% ±11/2> + 16.2% ±5/2>
5	298.2	1.514	3.154	13.987	28.0% ±11/2> + 27.0% ±3/2> + 21.1% ±1/2>
6	383.2	0.316	1.650	16.366	27.5% ±11/2> + 26.4% ±5/2> + 15.1% ±9/2>
7	420.8	0.045	1.386	16.344	40.3% ±9/2> + 28.5% ±7/2> + 9.7% ±11/2>
8	449.2	0.630	1.242	17.806	32.7% ±7/2> + 22.8% ±9/2> + 17.5% ±5/2>

Table S14. Calculated energy levels (cm^{-1}), \mathbf{g} (g_x , g_y , g_z) tensors and wavefunction compositions of the lowest eight Kramers doublets (KDs) of individual Dy1 fragments for compound **2**.

KDs	E/cm^{-1}	g_x	g_y	g_z	wavefunctions
1	0.0	0.006	0.021	19.648	97.57% ±15/2>
2	59.8	0.135	0.366	18.892	55.15% ±1/2> + 30.52% ±3/2> + 10.13% ±5/2>
3	161.7	2.104	2.700	14.059	27.79% ±3/2> + 22.85% ±5/2> + 15.54% ±1/2>
4	210.9	0.484	3.081	13.691	75.25% ±13/2> + 8.63% ±3/2> + 7.45% ±5/2>
5	261.0	9.011	7.035	4.485	21.34% ±5/2> + 20.48% ±7/2> + 17.10% ±1/2>
6	331.2	0.749	1.502	14.558	33.34% ±11/2> + 21.79% ±5/2> + 13.25% ±9/2>
7	371.9	0.070	0.177	18.547	33.48% ±11/2> + 30.77% ±9/2> + 24.94% ±7/2>
8	488.1	0.035	0.083	19.201	37.69% ±9/2> + 29.87% ±7/2> + 13.70% ±5/2>

Table S15. Calculated energy levels (cm^{-1}), \mathbf{g} (g_x , g_y , g_z) tensors and wavefunction compositions of the lowest eight Kramers doublets (KDs) of individual Dy2 fragments for compound **2**.

KDs	E/cm^{-1}	g_x	g_y	g_z	wavefunctions
1	0.0	0.004	0.007	19.767	99.20% ±15/2>
2	182.41	0.177	0.216	19.187	50.64% ±1/2> + 28.52% ±3/2> + 11.50% ±5/2>
3	275.27	0.226	0.474	15.302	86.67% ±13/2> + 3.93% ±1/2> + 2.96% ±7/2>
4	347.72	0.906	1.812	13.542	41.46% ±3/2> + 24.05% ±5/2> + 12.37% ±1/2>
5	411.36	8.256	7.834	4.236	25.14% ±11/2> + 24.38% ±5/2> + 19.92% ±1/2>
6	448.94	1.961	2.318	13.540	46.62% ±11/2> + 16.45% ±5/2> + 10.98% ±9/2>
7	540.53	1.312	2.727	14.468	41.63% ±7/2> + 30.44% ±9/2> + 16.86% ±11/2>
8	566.22	0.889	3.394	16.032	42.55% ±9/2> + 21.89% ±7/2> + 17.76% ±5/2>

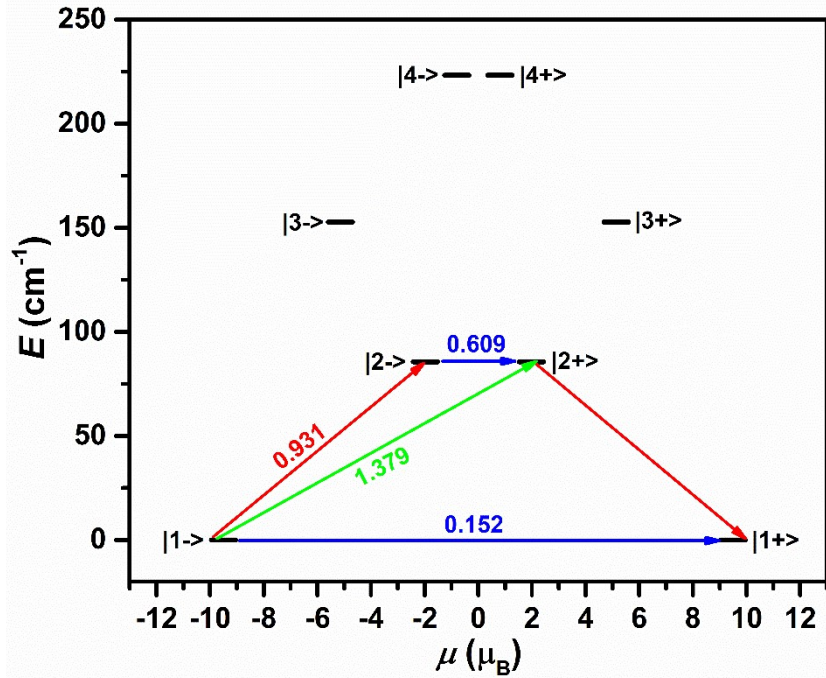


Fig. S7. Magnetization blocking barriers of individual Dy^{III} fragments in compound **1**. The thick black lines represent the KDs of the individual Dy^{III} fragments as a function of their magnetic moment along the magnetic axis. The blue lines correspond to diagonal matrix element of the transversal magnetic moment; the green line represents Orbach relaxation processes. The path shown by the red arrows represents the most probable path for magnetic relaxation in the corresponding compounds.

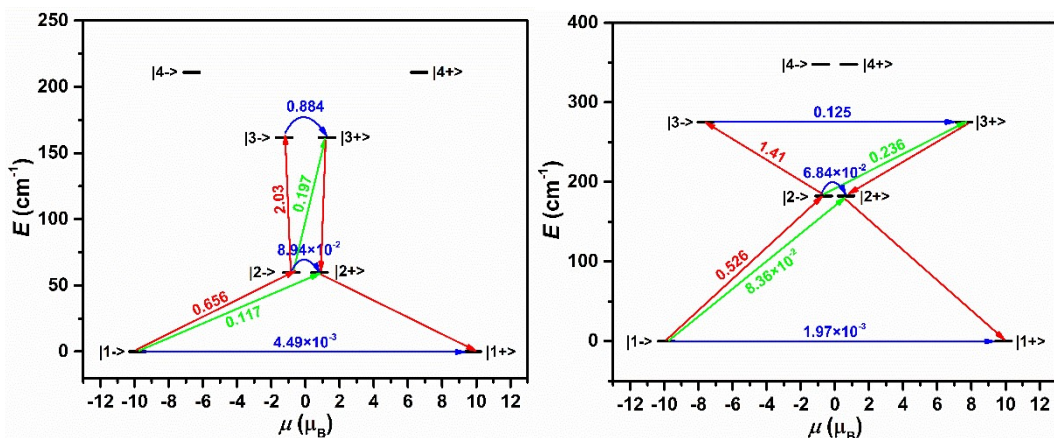


Fig. S8. Magnetization blocking barriers of individual Dy1 (left) and Dy2 (right) fragments in compound **2**. The thick black lines represent the KDs of the individual Dy^{III} fragments as a function of their magnetic moment along the magnetic axis. The blue lines correspond to diagonal matrix element of the transversal magnetic moment; the green line represents Orbach relaxation processes. The path shown by the red arrows represents the most probable path for magnetic relaxation in the corresponding compounds.

6. References

- 1 G. M. Sheldrick, *SADABS, Program for Siemens area detector absorption correction*, University of Göttingen, 1996.
- 2 O. V. Dolomanov, L. J. Bourhis, R. J. Gildea, J. A. K. Howard and H. J. Puschmann, *Appl. Crystallogr.*, 2009, **42**, 339–341.
- 3 (a) G. M. Sheldrick, *SHELXS97, Program for the solution of crystal structures*, University of Göttingen, Germany, 1997; (b) G. M. Sheldrick, *Acta Crystallogr., Sect. A: Fundam. Crystallogr.*, 2008, **A64**, 112–122; (c) T. Shiga, M. Ohba and H. Okawa, *Inorg. Chem. Commun.*, 2003, **6**, 15–18; (d) S. Akine, T. Matsumoto, T. Taniguchi and T. Nabeshima, *Inorg. Chem.*, 2005, **44**, 3270–3274.
- 4 O. Kahn, *Molecular Magnetism*, Wiley-VCH, New York, 1993.
- 5 F. Aquilante, J. Autschbach, R. K. Carlson, L. F. Chibotaru, M. G. Delcey, L. De Vico, I. Fdez Galvan, N. Ferre, L. M. Frutos, L. Gagliardi, M. Garavelli, A. Giussani, C. E. Hoyer, G. Li Manni, H. Lischka, D. Ma, P. A. Malmqvist, T. Muller, A. Nenov, M. Olivucci, T. B. Pedersen, D. Peng, F. Plasser, B. Pritchard, M. Reiher, I. Rivalta, I. Schapiro, J. Segarra-Marti, M. Stenrup, D. G. Truhlar, L. Ungur, A. Valentini, S. Vancoillie, V. Veryazov, V. P. Vysotskiy, O. Weingart, F. Zapata and R. Lindh, *J. Comput. Chem.*, 2016, **37**, 506–541.
- 6 L. Ungur and L. F. Chibotaru, *Chem. Eur. J.*, 2017, **23**, 3708–3718.
- 7 L. F. Chibotaru, L. Ungur, C. Aronica, H. Elmoll, G. Pilet and D. Luneau, *J. Am. Chem. Soc.*, 2008, **130**, 12445–12455.
- 8 L. Ungur, W. Van den Heuvel and L. F. Chibotaru, *New J. Chem.*, 2009, **33**, 1224–1230.